S. Afr. J. Chem., 2021, **75**, 6–17,
<https://journals.co.za/content/journal/chem/>.

Evaluation of Bitter Kola Leaf Extract as an Anticorrosion Additive for Mild Steel in 1.2 M H_2SO_4 Electrolyte

Valentine Chikaodili Anadebe[a,*] §, Patrick Chukwudi Nnaji[b], Nkechinyere Amaka Okafor[c], Joseph Okechukwu Ezeugo[c], Fidelis Ebunta Abeng[d] and Okechukwu Dominic Onukwuli[e]

[a]*Department of Chemical Engineering, Federal University Ndufu Alike, Ebonyi State, Nigeria.*
[b]*Department of Chemical Engineering, Michael Okpara University of Agriculture, Abia State, Nigeria.*
[c]*Department of Chemical Engineering, Chukwuemeka Odumegwu Ojukwu University, Nigeria.*
[d]*Material and Electrochemistry Unit, Department. of Chemistry, Cross River University of Technology, Calabar, Nigeria.*
[e]*Department of Chemical Engineering, Nnamdi Azikwe University Awka, Anambra State, Nigeria.*

Received 24 January 2020, revised 29 August 2020, accepted 29 August 2020.

ABSTRACT

Plant-based material, namely bitter kola leaf, as an additive for surface modification of mild steel in H_2SO_4 solution was thoroughly scrutinized using electrochemical, theoretical and optimization techniques. The functional groups, of the biomolecules of the bitter kola leaf extract, were examined using Fourier transform infrared spectrometry (FTIR) and gas chromatography-mass spectrophotometry (GC-MS). For clarification purpose, scanning electron microscopy (SEM) was used to inspect the texture of the degraded and inhibited steel after 21 h of immersion. For the response surface methodology (RSM), central composite design of Design-Expert Software was used to optimize the inhibition efficiency as a function of acid concentration, inhibitor concentration, temperature and time. The optimum inhibition efficiency of 93 % was obtained at 0.9 g L^{-1} bitter kola leaf. The mutual correlation between the considered variables and expected response was adequately interpreted by a quadratic model. The fitness of the model was justified by the following standards which include P-value (<0.0001), adjusted R^2 (0.9843), R^2 (0.991), adequate precision (43.14) and coefficient of variation (2.59). Bitter kola leaf extract behaved as a mixed-type inhibitor and adequately satisfied Langmuir adsorption isotherm. Furthermore, the theoretical modelling revealed the most active molecule of bitter kola leaf responsible for the overall inhibition. The experimental and theoretical results are in agreement that bitter kola leaf extract is a viable corrosion inhibitor of mild steel in H_2SO_4 solution.

KEYWORDS

Acid corrosion, electrochemical study, green extract, mild steel, optimization study, theoretical modelling.

1. Introduction

The continuous industrial development and the consequent use and generation of chemical complexes have resulted in the degradation of engineering process equipment through the corrosion process. In chemical industries, storage facilities and installation pipes are washed with acid solutions in high concentrations. Sometimes to eliminate the formation of clogging on the inside of transportation pipelines, they are treated with mineral acids like HCl and H_2SO_4. These mineral acids may cause severe corrosion in the storage facilities, pipes and oil reservoirs. Mostly, it is difficult to evaluate the level of internal corrosion that occurs at the bottom of the storage tanks. If the internal corrosion is not correctly monitored the effect or damage can be catastrophic. Therefore, this has necessitated the development of effective corrosion inhibitor in acidizing industries that can be mixed with mineral acids during routine treatment of industrial equipment.[1] A corrosion inhibitor is any substance that retards the rate of corrosion. The inhibitor is usually introduced in small dosages to the pickling acids in flow systems (pipes), either continuously or intermittently, to restrain corrosion attack on metallic materials.[2] The corrosion inhibitors retard the partial reactions through the formation of a dense film layer which functions as an impediment between corroding and the facial layer of the steel.[3] Organic compounds of plant-based material with chemical structures containing polyphenol, aromatic ring and heteroatoms are known to have inhibitive ability against corrosion of metals under hostile conditions.[4]

The high recommendation of plant-based materials is primarily because plant products are environmentally friendly and are widely accepted to minimize the cost of corrosion control.[5–6] Some researchers have classified bio-extracts, namely *Salvia officinalis* extract,[7] *Cuscuta reflexa* extract,[8] *Ficus tikoua* leaf extract,[9] Chinese gooseberry extract,[10] *Juglans regia* extract,[11] *Peganum harmala* seed extract [12] and Pigeon pea extract, as excellent inhibitive agents for steel in an acid medium.[13] However, some experts in corrosion mitigation have investigated bitter kola (*Garcinia*), especially the seed extract as corrosion inhibitor for mild steel in acid medium.[14–19] More so, in previous work[20] bitter kola leaf (BKL) extract demonstrated an inhibition efficiency of 90 % in HCl solution for mild steel corrosion. But there is a need to fill the gap in the bio-extract application as a corrosion inhibitor and synergistic contributions of the most active BKL molecules to the overall inhibition in H_2SO_4 environment using gas chromatography-mass spectrometry and density functional theory (DFT). Secondly, to model and optimize the inhibition efficiency by using response surface methodology.

The complex nature of biomolecules poses a significant hindrance to authenticate the actual constituents responsible for inhibition promotion. Consequently, efforts are geared towards

* To whom correspondence should be addressed.
E-mail: anadebechika@gmail.com / anadebe.valentine@funai.edu.ng

ISSN 0379-4350 Online / ©2021 South African Chemical Institute / http://saci.co.za/journal
DOI: https://doi.org/10.17159/0379-4350/2021/v75a2

the adoption of electronic and molecular analysis based on computer simulation using density functional theory (DFT) to theoretically analyze the impact of organic constituents on the overall inhibition process. In addition, response surface methodology (RSM), involving modelling and optimization, is a needed technique for convenient and efficient statistical analysis of the effects of the independent variables on the responses of the inhibition process.

Bitter kola, also known as *Garcinia kola*, is a species of flowering plant in the Clusiaceae or Guttiferae family. In Nigeria, it is abundantly grown in the eastern part of the country, especially in Anambra, Imo, Enugu, Abia and Ebonyi states. Bitter kola plants (their nuts, leaves, bark, fruit) offer a wide variety of useful elements, such as vitamins of the B-group, A, C and E, potassium, iron, fibre, calcium, and many antioxidants.[21] Bitter kola is highly recognized as a valuable plant due to the application of its phytochemicals in pharmaceutical industries.

2. Experimental Procedure

2.1. Preparation of BKL Extract

Fresh BKL samples were sourced from a bitter kola orchard at Uli farm in the Anambra State of Nigeria. The samples were air-dried for seven days in a conducive environment to eliminate the moisture content. The samples were ground into a powder to expose the extract constituents and increase the yield. The extraction method was carried out in batches. The separation procedure, as documented by Jeetendra *et al*.[22] was employed to obtain the extract. The liquid extract stock solution was stored at –4 °C until further use. The H_2SO_4 and ethanol used were of standard grade.

2.2. Metals Preparation

Corrosion studies were performed on mild steel of compositions P (0.02 %), Mn (0.11 %), Si (0.02 %), S (0.02 %), Cu (0.01 %), C (0.23 %), Ni (0.02 %), Cr (0.01 %) and Fe (99.56 %). At the commencement of the experiment, the mild steel was measured and mechanically cut. Each coupon was abraded with 220, 320 and 400 and 600 emery papers to obtain a good texture area. The coupons were rinsed with deionized water to eliminate organic impurities (oil and debris), degreased with acetone and preserved in a desiccator as previously explained.[22]

2.3. Characterization of BKL Extract

The GC-MS analyses were performed on a mass spectrometer Model No QP2010 plus from Shimadzu, Japan. The peaks in the chromatogram were scrutinized and compared with the database mass spectra stored in the GC-MS library to identify the bioactive constituents and chemical structures of the constituents in the BKL extract and test them as unique anti-corrosion agents. Further experiments involved titrimetric analysis in identifying the bioactive compounds in the BKL extract. Mild steel (MS) coupons were plunged in the inhibited medium. At the end of exposure, corrosion particles were scooped from the medium and mixed with KBr (potassium bromide) for FTIR study using a Shimadzu Model: IR Affinity-1 FTIR spectrophotometer. These analyses were done to understand the mechanistic process of inhibition through the functional groups present.

2.4. Weight-loss Method

The weight-loss method of the corrosion study was done at varying temperatures, as previously documented.[13,23] After the experiment, the samples were set aside, plunged in acetone and carefully re-assessed. The data were noted sequentially and scrutinized by using Equations (1), (2), (3), and (4) as adopted from literature.[24]

$$\Delta w = w_i - w_f \quad (1)$$

$$C_R = \frac{w_{bl} - w_{inh}}{A(m^2) \times t(day)} \quad (2)$$

$$IE\% = \frac{w_{bl} - w_{inh}}{w_{bl}} \times 100 \quad (3)$$

$$\theta = \frac{w_{bl} - w_{inh}}{w_{bl}} \quad (4)$$

where Δw represents the weight-loss, with w_i and w_f the initial and final weights of the coupons, respectively, and w_{bl} and w_{inh} the weigth-loss values obtained in the unprotected and protected environments. A is denoted as the entire area of the steel and t represents the time duration of the study.

2.5. Activation and Heat of Adsorption

By considering the corrosion rates of the mild steel at T_1 and T_2 as C_{R_1} and C_{R_2}, Equation (5) was used to evaluate and predict the activation energy. The heat of adsorption Q_{ads} (kJ mol^{-1}) was calculated using Equation (6).

$$\ln(C_{R_2} / C_{R_1} = \left(\frac{E_a}{2.303R}\right)\left(\frac{1}{T_1} - \frac{1}{T_2}\right) \quad (5)$$

$$Q_{ads} = 2.303R\left[\log\left(\frac{\theta_2}{1-\theta_2}\right) - \log\left(\frac{\theta_1}{1-\theta_1}\right)\right] \times \frac{T_2 - T_1}{T_2 - T_1} \quad (6)$$

where E_a is the activation energy, R denotes the gas constant and, θ_1 and θ_2 represent the degree of surface coverage at temperature T_1 and T_2. θ_1 and θ_2 were evaluated using Equation (4) of Section 2.4.

2.5.1. *Adsorption Models*

The experimental data and surface coverage were fitted into the Langmuir, Frumkin, Temkin and Flory-Huggins isotherms as represented by Equations (7), (8), (9) and (10), respectively:

$$\frac{C}{\theta} = \frac{1}{K_{ads}} + C \quad (7)$$

$$\log\left[(C) \times \left(\frac{\theta}{1-\theta}\right)\right] = 2.303\ \log K + 2\alpha\theta \quad (8)$$

$$\theta = \frac{2.303 \log K}{2a} - \frac{2.303 \log C}{2a} \quad (9)$$

$$\log\left[\left(\frac{\theta}{C}\right)\right] = \log K + x \log(1-\theta) \quad (10)$$

C represents the concentration of BKL, K_{ads} denotes the adsorption equilibrium constant, α is the mutual interaction term explaining the nature of the adsorbed layer, a is the attractive parameter, and x is the size parameter. (This evaluates the dosage of the adsorbed H_2O molecules sub-planted by BKL molecules.)

Then the Gibbs energy of adsorption (ΔG_{ads}) was evaluated from Equation (11).

$$\Delta G_{ads} = -2.303RT\log(55.5K) \quad (11)$$

2.6. Electrochemical Test

A standard electrochemical test was performed using a VERSASTAT 400 full set DC Voltammetry and Corrosion System, with V3 Studio software. The electrochemical impedance study was carried out over a frequency range of 100 kHz–10 MHz with

a signal amplitude perturbation of 10 mV. The potentiodynamic/galvanostat corrosion system with E-chem software was used. The polarization study, considering ±250 mV *versus* E_{corr} and a scanning rate of 0.333 mV s^{-1}. Mild steel of 1 cm^2 was used as the main electrode. To investigate the effect of the optimum and minimum concentration of BKL extract on mild steel in 1.2 M H_2SO_4 and 0.3 M H_2SO_4, varying concentrations of 0.3 g L^{-1} and 0.9 g L^{-1} BKL were used. All data were measured in triplicate for reproducibility of average values and further statistical analysis. The inhibition efficiency was evaluated by using Equation (12).

$$IE\% = \frac{i_{corr(bl)} - i_{corr(inh)}}{i_{corr(bl)}} \times 100 \quad (12)$$

where $i_{corr(bl)}$ and $i_{corr(inh)}$ are the current density values in the absence and presence of inhibitor.

2.7. Quantum Chemical Calculations

Quantum chemical calculations were performed using the DFT electronic structure programs VAMP and DMol[3] as contained in Materials Studio 4.0 software. The Fe slab for the simulations was cleaved along the (110) plane. The calculations were performed in a 12 × 10 super cell using a compass force field and the smart algorithm with NVE (micro canonical) ensemble, a time step of 1 fs and simulation time of 5 ps. The temperature was fixed at 303 K. The system was quenched automatically at intervals of 250 steps.

3. Results and Discussion

3.1. GC-MS Characterization of BKL Extract

The gas chromatography-mass spectrometric analysis of the ethanol extract of BKL is shown in Fig 1. Each of the peaks was evaluated and authenticated. The peaks signify different compounds present in the BKL extract. The compounds include fatty acids, aromatics, esters, alcohols and phenols. The most dominant compounds were undecene at peak three and ascorbic acid at peak 7, which were isolated. Other compounds revealed by the BKL chromatogram, included pentadecanoic acid, 14-octadecenoic acid, allyl nonanoate, 9-tetradecenal, myristoleic acid and hexadecanoic acid.

3.2. Phytochemical Screening

Table 1 presents the active constituents of the BKL extract. It revealed various levels of phytochemicals present in the extract. A standard titrimetric method was used to identify the active ingredients present in the BKL extract. These active ingredients were seen to associate with *garcinia bio-flavonoids*, a mixture known as *kolaviron*. The active ingredients have anti-inflammatory and anti-oxidant characteristics,[25] which prove the anti-corrosion performance of the BKL extract. Polyphenolic compounds like flavonoids and phenolic acids, usually exist in large quantities in dried leaves.[25] Flavonoids naturally exist in plant-based materials as a response to microbial disease and have a benzo-γ-pyrone ring structure.[26] Phenolics are a group of compounds obtained from hydroxycinnamic and hydroxybenzoic acids that exist in dry plants or leaves containing enough gallic acid as the major constituent.[27] Alkaloids are a class of constituents that contain some basic nitrogen atoms, like 4′-hydroxyphenylethanamide-α-L-rhamnopyranoside, N, α-L-rhamnopyranosyl vincosamide and phenyl acetonitrile pyrrole-marumine derivatives.[28] The green pigment (carotenoid) from BKL extract has a bitter taste due to the high composition of tannins and different complexes of compounds such as 'triterpenes'. Tannins are known to contain polyphenolic moieties which form tanninate salts with ferric ions. The inhibition activity of tannins is attributed to the formation of a dense cross-linked film of ferric tanninate salts that shield the steel surface.[29] Also, triterpenes contain some vital functional groups which are diagnostic markers of aliphatic and aromatics families. BKL are a good source of saponins that are covalently

Table 1 Bioactive constituents of BKL extract.

Active compounds	Qualitative	Quantitative/mg100 g^{-1}
Flavonoids	++	763
Alkaloids	++	1355
Phenolics	+++	124
Phytates	++	73
Saponins	++	80
Tannins	++	940
Cardiac glycosides	+	213

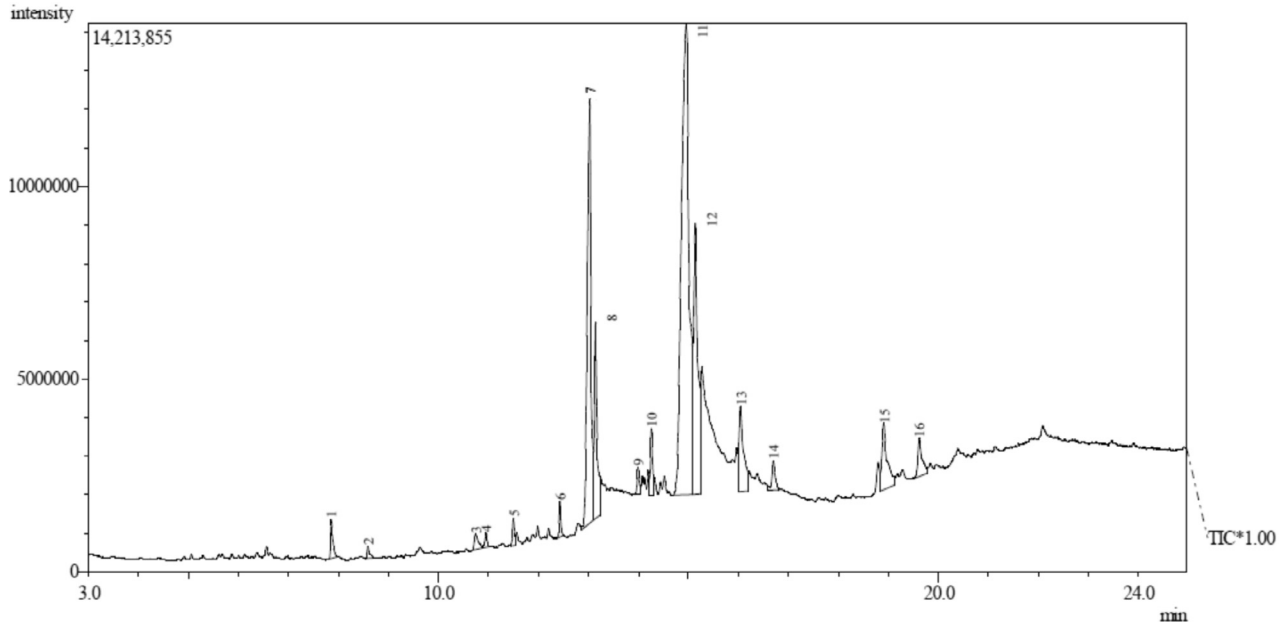

Figure 1 Chromatogram of BKL extract.

connected to one or complex sugar moieties.[30] Saponins serve as an antidote for the treatment of cancer.

3.3. FTIR Analysis of BKL Extract and Corrosion Product

The active functional groups in the BKL constituents behind the surface attachment and aiding the impeding of corrosion of mild steel were obtained through FTIR analysis. The results of the FTIR analyses of BKL extract and corrosion products in 1.2 M H_2SO_4 are shown in Table 2. The crude BKL sample before corrosion revealed a variety of peaks wave numbers. By scrutinizing the values with FTIR data, different categories of functional groups were identified. Most of the peaks authenticated in the crude BKL sample also existed in the adsorbed film (presence of BKL extract), some peaks slightly deviated from their initial positions. Some of the peaks completely vanished, showing that they have been used up during the inhibition mechanism. But, some of the peaks, such as O-H around (3674.48 cm^{-1}) and NO_2 stretch of nitro compound (1381.64 cm^{-1}), remained unchanged and stable. As presented in Table 2, the functional groups of N-H, C-H, C=O, C-N, and C-O recorded significant change in peaks and intensities, which signify that they took part during the inhibition process. The nitrogen and oxygen atoms of BKL molecules spontaneously accumulated on the facial layer of the steel, forming a dense film which prevented the ingress of the electrolyte onto the steel surface.[31–32]

3.4. Result of Weight-loss Method

Table 3 presents the experimental results of the weight-loss (gravimetric) method. It revealed the level of variations of weight-loss, corrosion rate, inhibition efficiency and degree of surface coverage with time, temperature and inhibitor concentration in 1.2 M H_2SO_4. The inhibition efficiency increased with increments in the inhibitor concentration. The presence of BKL in the electrolyte medium caused significant retardation of corrosion. This observation is in agreement with previous reports.[33–34] An increased inhibitor concentration increases the rate and quantity of active extract for the surface attachment on the degrading metal surface.[35] The surface coverage declined with an increase in temperature because a temperature rise agitates the system, thereby minimizing the level of adsorption of the inhibitor's species on the mild steel. The level of surface coverage relied on the increase of the surface fraction occupied by the molecules of the plant extract. The results revealed that BKL is a suitable additive in surface treatments or modification of metals in H_2SO_4 medium.

3.5. Activation Energy (E_a) and Heat of Adsorption (Q_{ads}) Studies

The parameters E_a and Q_{ads} for protection of mild steel in H_2SO_4 with BKL extract are shown in Table 4. The values of the activation energy obtained indicated that adsorption of BKL extract on the metal surface is by the phenomenon of physical adsorption. In all, the heat of adsorption is negative, implying that the attachment of the active species of BKL on the steel surface is exothermic, stable and spontaneous.

Table 3 Gravimetric results of mild steel in 1.2 M H_2SO_4 with BKL.

Time/h	Temp/K	IC/g L^{-1}	Weight-loss/g	CR/mm y^{-1}	IE/%
21	300	0.0	1.79		
		0.3	0.74	1.762	58.66
		0.6	0.51	1.214	71.51
		0.9	0.29	0.690	93.00
	312	0.0	1.83	4.357	
		0.3	0.79	1.881	56.83
		0.6	0.62	1.476	66.12
		0.9	0.43	1.024	76.50
	324	0.0	1.88	4.476	
		0.3	0.94	2.238	50.00
		0.6	0.65	1.548	65.43
		0.9	0.48	1.143	74.47
14	300	0.0	1.32	4.714	
		0.3	0.59	2.107	55.30
		0.6	0.41	1.464	68.94
		0.9	0.27	0.964	80.55
	312	0.0	1.51	5.393	
		0.3	0.72	2.571	52.32
		0.6	0.54	1.929	64.24
		0.9	0.37	1.321	75.50
	324	0.0	1.69	6.036	
		0.3	0.87	3.107	48.52
		0.6	0.63	2.250	62.72
		0.9	0.44	1.571	73.96
7	300	0.0	0.95	6.786	
		0.3	0.51	3.643	46.32
		0.6	0.34	2.249	64.21
		0.9	0.22	1.571	76.84
	312	0.0	1.08	7.714	
		0.3	0.59	4.214	45.37
		0.6	0.49	3.500	54.63
		0.9	0.30	2.143	72.22
	324	0.0	1.17	8.357	
		0.3	0.74	5.286	36.75
		0.6	0.55	3.929	52.99
		0.9	0.37	2.643	68.38

3.5.1. *Adsorption Study*

In corrosion studies, it is believed that the control of metal corrosion takes place due to adsorption of plant molecules. The dominant adsorption type will be dependent on factors such as heterocyclic constituents of the extract, chemical changes to the

Table 2 FTIR analysis of BKL extract in 1.2 M H_2SO_4.

BKL extract	Corrosion product in 1.2 M H_2SO_4 with 0.9 g L^{-1} BKL
3674.48 cm^{-1} -O-H stretch of alcohols	3674.48 cm^{-1} - O-H stretch of alcohols
3384.98 cm^{-1} -N-H stretch of primary amines	3481.48 cm^{-1} - N-H stretch of primary amines
3045.30 cm^{-1} - C-H stretch of alkanes	2860.02 cm^{-1} - C-H stretch of aldehydes
2805.98 cm^{-1} -C-H stretch of aldehydes	1954.92 cm^{-1} - C=O stretch of carboxyl group
1968.36 cm^{-1} - C=O stretch of carboxyl group	1748.34 cm^{-1} - C=O aldehydes
1748.34 cm-^{1} - C=O aldehydes	1381.64 cm^{-1} - NO_2 stretching nitro
1381.64 cm^{-1} - NO_2 stretching nitro	1204.08 cm^{-1} - C-N stretch aliphatic amines
1227.24 cm^{-1} - C-N stretch of aliphatic amines	1068.98 cm^{-1} - C-O stretch of ethers
1007.22 cm^{-1} – C-O stretch of ether	

Table 4 Activation energy and heat of adsorption.

Inhibitor concentration	E_a/kJ mol^{-1}	Q_{ads}/kJ mol^{-1}
0.0	38	–
0.2	52	–25
0.3	51	–28
0.6	53	–28
0.9	57	–30

extract and the interaction of the surface charge on the metal. Various adsorption isotherms have been tested. The experimental data were fitted into the Langmuir, Frumkin, Temkin and Flory-Huggins adsorption isotherms which are presented in Figs. 2–5, respectively. The Langmuir adsorption isotherm produced the best fit with the experimental data using Equation (7).

The plot of log C/θ *versus* log C gave a straight-line graph, with clear values of the slope and intercept. The correlation of determination (R^2) (0.9918) gave the extent of correlation between the experimental data and isotherm equations, as seen in Table 5. The strong adherence to the Langmuir adsorption isotherm is in accordance with previous reports.[36–37] It suggests a mutual relationship between the BKL molecules and surface fractions of the mild steel. Comparing the equations in Figs. 2–5 with the isotherm equations, the adsorption properties K, α, a and x were generated, the surface interaction (α) is positive proving a unique action of BKL on the degraded steel. The value (a) assumes significant coverage when the increase of BKL thickness is high for non-uniform steel, and the mode of attachment is negligible. The range of (x) is positive proving that the surface attachment of active species is bulky.

Table 5 Adsorption parameters for the corrosion of mild steel in 1.2 M H_2SO_4 with BKL.

Adsorption	Temp./K	R^2	log K	ΔG_{ads} /kJ mol^{-1}	Isotherm
Langmuir	300	0.991	–0.083	–9.54	–
	324	0.988	–0.138	–9.97	–
Frumkin	300	0.980	–1.313	–2.48	α 2.312
	324	0.952	–1.297	–2.77	2.224
Temkin	300	0.918	–2.119	2.20	a–3.656
	324	0.872	–2.292	3.40	–2.998
Flory-Huggins	300	0.787	0.822	–14.74	x 1.763
	324	0.757	0.909	–16.46	1.172

3.6. Potentiodynamics Polarization

Results of the potentiodynamic polarization study of the corrosion are shown in Fig. 6. A thorough examination of the plots revealed that in 1.2 M H_2SO_4 and 0.3 M H_2SO_4 acid concentrations, the existence of BKL in the test solution pushed the anodic and cathodic side to the minimum current values.[38] It is evident that the BKL extract obstructed the anodic and cathodic sites from further reactions. The electrochemical variables, namely corrosion potential E_{corr}, and corrosion current densities i_{corr} generated from this experiment are listed in Table 6. The immersion of BKL in 1.2 M H_2SO_4 gently pushed E_{corr} to the anodic direction compared to the unprotected medium, while in 0.3 M H_2SO_4 the shifting mechanism in E_{corr} was not pronounced. The inconsistency in β_c and β_a values in the H_2SO_4 environment decreased slightly upon the immersion of BKL extract, which indicates corrosion inhibition promotion. The

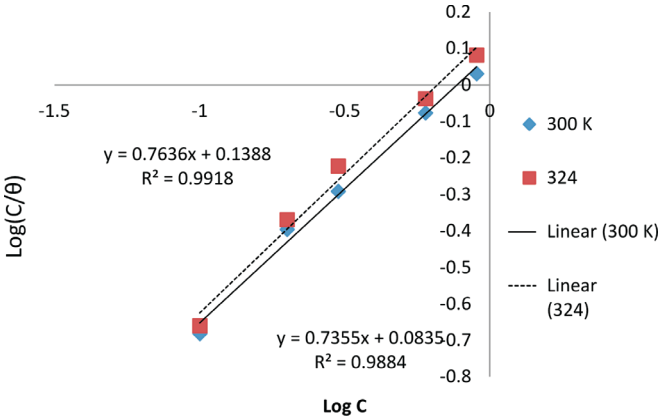

Figure 2 Plot of the Langmuir isotherm for mild steel in H_2SO_4 with BKL.

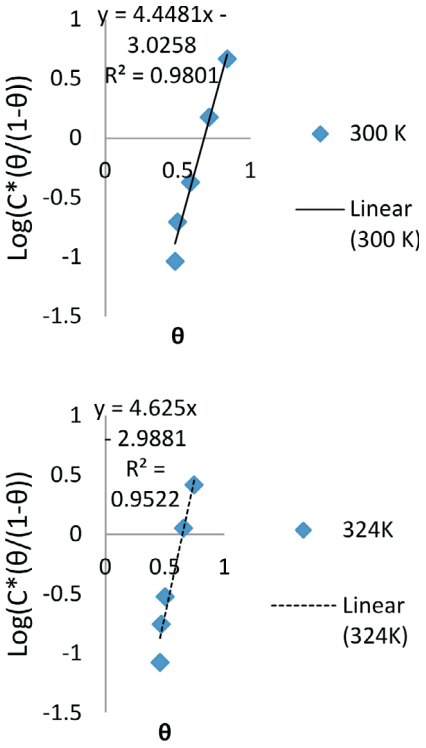

Figure 3 Plot of Frumkin isotherm for mild steel in H_2SO_4 with BKL.

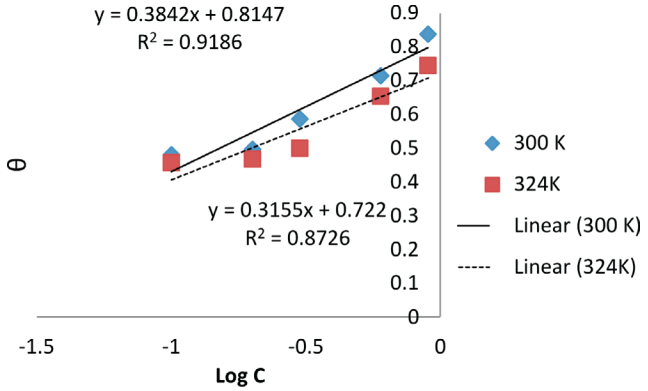

Figure 4 Plot of Temkin isotherm for mild steel in H_2SO_4 with BKL.

phenomenon of inhibition is due to synergistic action. In general, a situation where the shift in E_{corr} is above 85 mV, the inhibitor can be categorized in the rank of anodic or cathodic and if the shift is lower than 85 mV the inhibitor may be seen as a mixed-type inhibitor.[39] The results of this study revealed that the

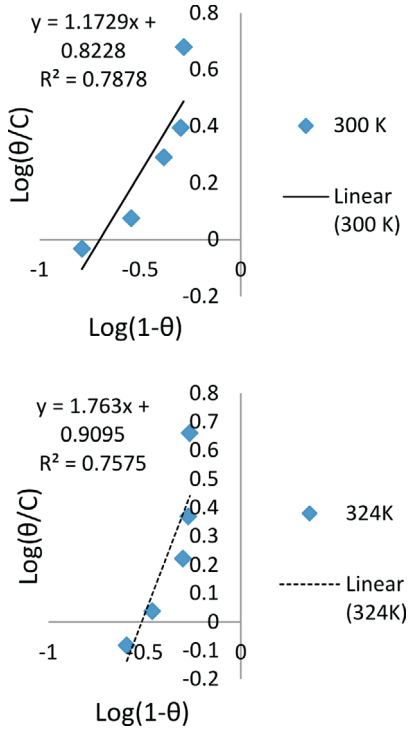

Figure 5 Plot of Flory-Huggins isotherm for mild steel in H_2SO_4 with BKL.

Table 6 Parameters from Tafel polarization measurements.

System	E_{corr} /mV *vs.* SCE	I_{corr} /μA cm^{-2}	β_c /mV dec^{1}	β_a /mV dec^{-1}	IE /%
1.2 M H_2SO_4/BKL	–496.4	1340	90	44.2	–
0.3 g L^{-1}	–478.6	778.9	92.6	55.3	41.9
0.9 g L^{-1}	–489.2	115.4	91.5	41.4	90.1
0.3 M H_2SO_4/BKL	–463.9	728.4	86.6	58.9	–
0.3 g L^{-1}	–459.8	475.2	98.3	55.1	34.8
0.9 g L^{-1}	–463.2	90.6	97.6	52.5	87.6

phenomenon of the inhibition is a mixed-type corrosion control, with inhibition of both cathodic and anodic reactions.[40] Also, at elevated voltages that are greater than *circa* –350 mV (SCE), it was observed that metal dissolution was greater than BKL adsorption.

3.7. Electrochemical Impedance Study

Impedance measurements were performed to evaluate the characteristics and kinetics of the metal/solution interface and how the reaction was obstructed by the BKL extract. Fig. 7 shows the Nyquist plots of mild steel in the devoid off and inhibited solution. The obtained plots consist of a single imperfect circle in the high-frequency region.[41–42] The observed decrease in the Nyquist plots with the middle under the real axis is typical for solid metal electrodes that show frequency dispersion of the

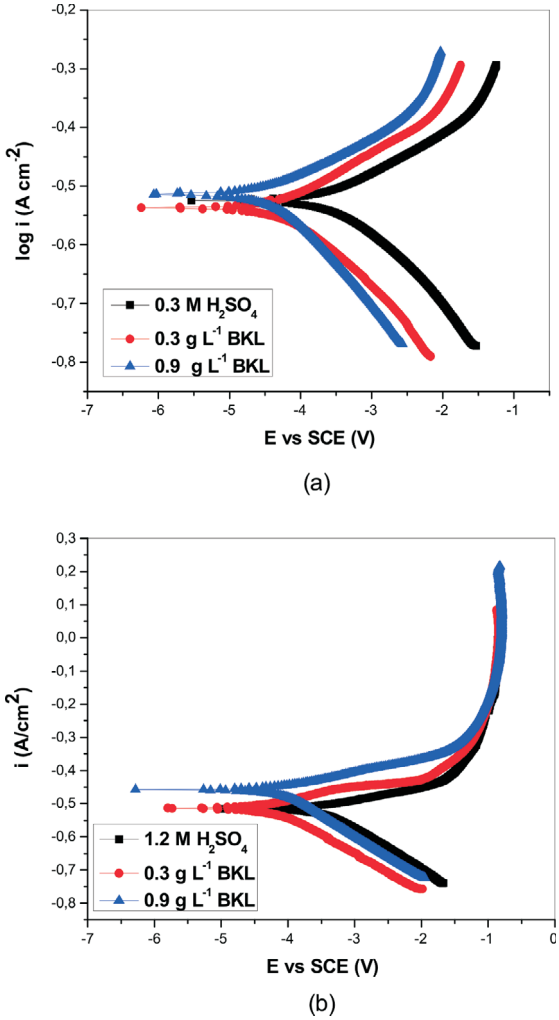

Figure 6 Potentiodynamic polarization plots of mild steel in (**a**) 1.2 M H_2SO_4 and (**b**) 0.3 M H_2SO_4 in the absence and presence of BKL.

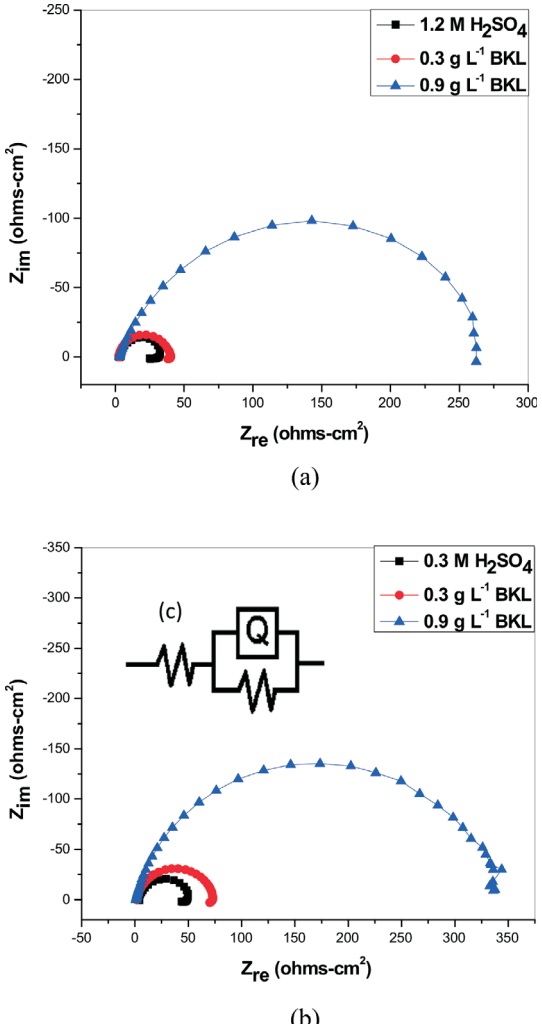

Figure 7 Impedance spectra of mild steel in (**a**) 1.2 M H_2SO_4 and (**b**) 0.3 M H_2SO_4 solution in the absence and presence of BKL extract, and (**c**) equivalent circuit.

impedance data. It can be attributed to coarseness and surface fractions of the metal.[43–44] Constant phase element (CPE) is employed to substitute a capacitor to envisage the shifting mechanism due to the dark densely flakes on the electrode. The impedance of the CPE is denoted by:[38]

$$Z_{CPE} = Q^{-1}(jw)^{-n} \quad (13)$$

where Q and n are associated with CPE and exponent, respectively, $j^2 = -1$ is regarded as the imaginary axis, ω stands for angular frequency in rads^{-1}, ($\omega = 2\pi f$ explains the frequency in H_Z), R_S signifies solution resistance, W denotes the impedance factor and n is the considered shifting factor which explains the surface heterogeneity, impurities and surface fractions of the metal.[45]

Addition of BKL extract in the blank solution assisted in promoting the radius of the imperfect circle, which denotes the impeding of the corrosion, and it corresponds to R_{ct} of the steel surface. Also, an increase in BKL from 0.3 g L^{-1} to 0.9 g L^{-1} promotes the radius of the impedance response, but no drastic effect is seen. As listed in Table 7, it is apparent that in the case of the inhibitor-containing H_2SO_4 solution, the increase in BKL concentration led to a deviation or reduction in the n-value. On the contrary, for the sample immersed in blank H_2SO_4, the reduction is not attributed to the rise in coarseness or impurities on the surface. The irregularity in the n value obtained is because of the increase in surface heterogeneity due to the spontaneous attachment of BKL molecules on the steel surface. Also, the R_{ct} values were enhanced from 28.1 to 265 Ω cm^2 in 1.2 M H_2SO_4 and 50 to 345.2 Ω cm^2 in 0.3 M H_2SO_4 at the optimum concentration of 0.9 g L^{-1}. In the same vain, C_{dl} is another vital parameter considered in the EIS study, C_{dl} experiences a significant shift/reduction in the protected environment and declines consistently with BKL concentration. This decline denotes that BKL acts by adsorption on the metal/solution interface by substituting water molecules with BKL molecules, forming a dense film layer on the metal surface.[46–50] This is following Helmholtz's law. Furthermore, the mechanistic interpretation of the trend of corresponding C_{dl} values in metal/H_2SO_4 explains the compactness of the BKL thin layer within 24 hours.

Table 7 Impedance parameters of mild steel in H_2SO_4.

System	Rs /Ω cm^2	R_{ct} /Ω cm^2	n	C_{dl} /F cm^2	IE /%
1.2 M H_2SO_4/BKL	2.061	1340	0.90	1.131E-4	–
0.3 g L^{-1}	2.89	778.9	0.88	5.144E-5	40.2
0.9 g L^{-1}	3.25	115.4	0.86	4.371E-5	90.4
0.3 M H_2SO_4/BKL	2.173	728.4	0.89	3.987E-5	–
0.3 g L^{-1}	3.46	475.2	0.88	2.672E-5	33.7
0.9 g L^{-1}	4.01	90.6	0.87	2.238E-5	85.5

3.8. Theoretical Modelling

The major purpose for the computational study is not only to throw more light on the adsorption of the BKL extract but to further identify the contribution of a specific extract constituent through its adsorption phenomenon and energy. Density functional theory (DFT) calculations were carried out to design the electronic and adsorption structures of undecene (UD) and ascorbic acid (AA) as shown in Fig. 8 which was the main chemical constituents of the BKL extract. The constituents were analyzed by DFT electronic structure software DMol^3 using a Milliken population test.[51]

The study embraces the simulation of molecular electronic structures involving frontier molecular orbitals and Fukui

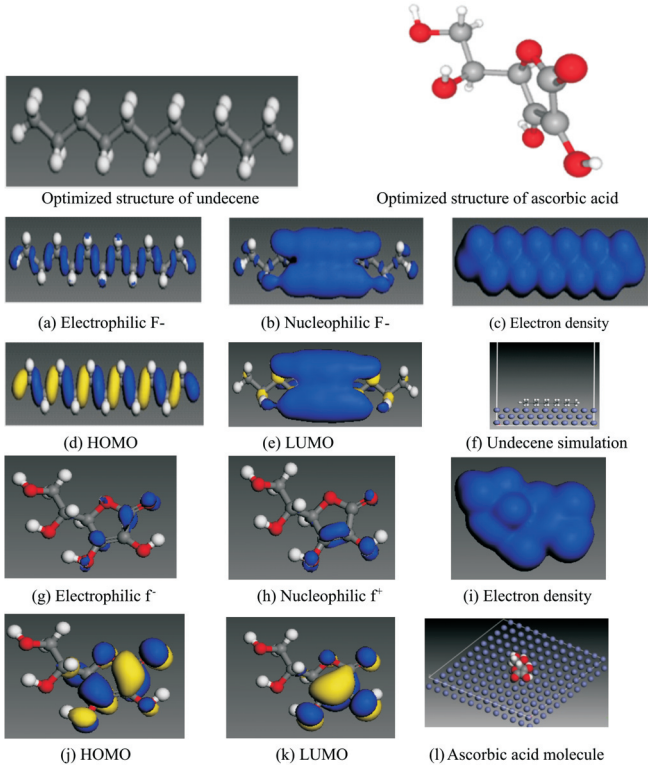

Figure 8 Undecene molecule: (**a**) Electron density, (**b**) Electrophilic f–, (**c**) Nucleophilic f +, (**d**) HOMO, (**e**) LUMO, (**f**) attachment of undecene molecule on Fe (110). Ascorbic acid molecule: (**g**) Electrophilic f–, (**h**) Nucleophilic f+, (**i**) Electron density (**j**) HOMO, (**k**) LUMO, (**l**) attachment of ascorbic acid on Fe surface (110).

indices to ascertain the active compounds in the BKL molecules. As previously expressed,[52–53] the areas of highest electron density (HOMO) denote the sites at which electrophiles attack and the active points where adsorption takes place at the metal surface. At the same time, the LUMO orbital receives electrons from the metal with the help of anti-bonding orbitals to form barriers.

With the Fukui analysis, it is easier to accelerate the reactive areas in terms of electrophilic (f–) and nucleophilic (f+) attack. E_{HOMO} is often associated with the electron-donating ability of a molecule, while E_{LUMO} shows its electron-accepting ability. According to the results presented in Table 8, the higher energy value of E_{HOMO} reveals the ability of a molecule to donate an electron to an empty molecular orbital. Thus, an increase in the E_{HOMO} value facilitates adsorption of an inhibitor, while the energy of LUMO shows the potential of the molecule to accept electrons.[54–55] The energy gap can also be used to predict the inhibition efficiency of a compound or to develop a theoretical model for explaining the structure and confirmation barrier in many molecular systems. In the same vain, minimum values obtained from the energy gap $E_{LUMO–HOMO}$ gives a unique inhibition efficiency since the energy to displace an electron from the last occupied orbital will be reduced to the barest minimum.[56–59] Energy gap (ΔE) is calculated by using the Equation (14):

$$\Delta E = E_{LUMO} - E_{HOMO} \quad (14)$$

From our study, the value of ΔE in Table 8 is within the range of values of suitable corrosion inhibitors. Also, the electronegativity reflects the power of an electron or group of atoms to attract electrons toward itself. The Koopman's theorem was used to estimate the electronegativity (χ) of the studied compound using the following Equation (15):

Table 8 Quantum chemical calculations for undecene and ascorbic acid.

Molecule	E_{HOMO}/eV	E_{LUMO}/eV	ΔE/(eV)	χ/eV	η/eV	σ	ΔN/e	Molecular mass	E_{bind}/kcal mol^{-1}
Undecene	–6.906	–1.905	5.001	4.4055	2.5005	0.3999	0.1629	170	–113.1
Ascorbic acid	–5.319	–1.647	3.672	3.4830	1.8360	0.5446	0.3641	176	–40.5

$$\chi = -\tfrac{1}{2}(E_{HOMO} - E_{LUMO}) \quad (15)$$

The higher the value of χ, the more effective is the inhibitor and *vice versa*. Data in Table 8 show that the χ value is within the range of effective inhibitors. These results agree with the experimental results of other studies.[60]

The global hardness (η) measures the resistance of an atom to charge transfer. In contrast, the global softness (σ) describes the capacity of an atom or group of atoms to receive electrons. The expressions for η and σ are given as follows:

$$\eta = -\tfrac{1}{2}(E_{HOMO} - E_{LUMO}) \quad (16)$$

$$\sigma = -\frac{1}{\eta} \quad (17)$$

A hard molecule requires a large ΔE and a soft molecule requires a small ΔE. Soft molecules could, therefore, easily offer electrons to an acceptor system that makes them more reactive than hard molecules. Furthermore, adsorption may occur at the point of a molecule where absolute softness is high. Table 8 shows that the values of global hardness and global softness are within the range of effective corrosion inhibitors.

The fraction of transferred electrons (ΔN) can be evaluated by using the following Equation (18):

$$\Delta N = \frac{W - \chi_{inh}}{2(\eta_{Fe} + \eta_{inh})} \quad (18)$$

where W is a work function, χ_{inh} is the electronegativity of inhibitor, while η_{Fe} and η_{inh} are the global hardness of Fe and the inhibitor, respectively. The electronegativity χ was calculated by using Equation (13), the value of η_{Fe} was taken as 0 eV mol^{-1}, while η_{inh} was calculated using the global hardness equation. To calculate ΔN, the work function with the value of W = 4.82 for Fe (110) mild steel surface was applied. For the value of ΔN > 0, the electron transfer takes place between an inhibitor molecule and the metal surface. In contrast, for ΔN < 3.6, the electron-donating ability of an inhibitor molecule is increased. All the calculated values of this study are within the range of values already reported for some excellent corrosion inhibitors.[61] This investigation revealed the most active molecule, but this does not mean that other active compounds do not participate in the inhibition phenomenon. The overall inhibitive action of BKL is due to the synergistic attachment of the various active molecules, and the charge transfer process is saturated across the active molecules, and a flat-lying adsorption phenomenon is observed.

Furthermore, the phytochemical nature of these active molecules is a very important area of research. Undecene is an alkene that is *undecane* containing one double bond located at position 1. It has a role as a plant metabolite. The HOMO emerges overall carbonyl and nitrogen heteroatoms while the carbon atoms and other aromatics acted as LUMO. For ascorbic acid, the C=C bond (5-membered ring ether O atom, carbonyl and OH oxygen atoms fused to ring) acted as major areas of HOMO. In contrast, the C areas (contain 5-membered ring with double bond ether oxygen or its closest O atoms) behaved as regions of LUMO,[6] indicating the synergistic efforts of the *garcinia bio-flavonoids* family in the inhibition study.

Mathematically, to evaluate the mutual interaction between the BKL molecules and the Fe (110), the adsorption energy (E_{ads}) of each system was calculated using Equation (19).

$$E_{interact} = E_{total} - (E_{BKL} + E_{Ms}) \quad (19)$$

E_{total} denotes the energy of the molecular simulation BKL and MS surface, E_{BKL}, $E_{Ms,}$ and E_{total} reveals the strength of one molecule on the Fe slab (110).

3.9. Result of Weight-loss Method using Response Surface Methodology

The design of an experiment is a systematic approach, before experiments that considers all factors involved simultaneously. It helps to analyze and pinpoint the sensitive areas in design that affect the desired response. Results of a 30-run experiment showing the interactive nature of the considered factors on the responses of the inhibition process are presented in Table 9.

3-D plots are presented in Fig. 9. The predicted *versus* actual plots generated a linear graph, implying that the obtained model gives adequate fitting with the experimental data (Fig. 9a).[62–63] The characteristics of the 3-D plots (Fig. 9b–e) showed that there is good coordination among the factors of the corrosion inhibition process. Fig. 9b indicated that there is mutual interaction between temperature and inhibitor concentration. The

Table 9 Design of experiment (CCD) with their expected responses.

Std.	Exp. run	AC /M	IC /g L^{-1}	T /K	Time /h	Wt. loss /g	CR /mm y^{-1}	IE /%
5	1	0.30	0.3	324	7	0.76	5.429	35.04
6	2	1.20	0.3	324	7	0.74	5.286	36.74
27	3	0.75	0.6	312	14	0.43	1.536	67.42
17	4	0.30	0.6	312	14	0.44	1.571	53.68
28	5	0.75	0.6	312	14	0.43	1.536	67.42
30	6	0.75	0.6	312	14	0.43	1.536	67.42
2	7	1.20	0.3	300	7	0.51	3.643	46.32
13	8	0.30	0.3	324	21	0.84	2	38.69
15	9	0.30	0.9	324	21	0.40	0.952	70.8
14	10	1.20	0.3	324	21	0.94	2.238	50
1	11	0.30	0.3	300	7	0.52	3.714	45.26
16	12	1.20	0.9	324	21	0.48	1.143	74.47
3	13	0.30	0.9	300	7	0.23	1.643	75.79
22	14	0.75	0.6	324	14	0.56	2	64.33
8	15	1.20	0.9	324	7	0.37	2.643	68.38
10	16	1.20	0.3	300	21	0.74	1.762	58.66
12	17	1.20	0.9	300	21	0.29	0.690	93
18	18	1.20	0.6	312	14	0.54	1.929	64.42
19	19	0.75	0.3	312	14	0.62	2.214	72.73
25	20	0.75	0.6	312	14	0.43	1.536	66.67
21	21	0.75	0.6	300	14	0.33	1.179	51.35
7	22	0.30	0.9	324	7	0.39	2.786	66.67
9	23	0.30	0.3	300	21	0.54	1.286	51.35
24	24	0.75	0.6	312	21	0.50	1.19	69.51
11	25	0.30	0.9	300	21	0.27	0.643	75.68
4	26	1.20	0.6	300	7	0.23	1.571	76.84
26	27	0.75	0.6	312	14	0.43	1.536	67.42
20	28	0.75	0.9	312	14	0.28	1	78.79
29	29	0.75	0.6	312	14	0.43	1.536	67.42
23	30	0.75	0.6	312	7	0.38	2.714	60.82

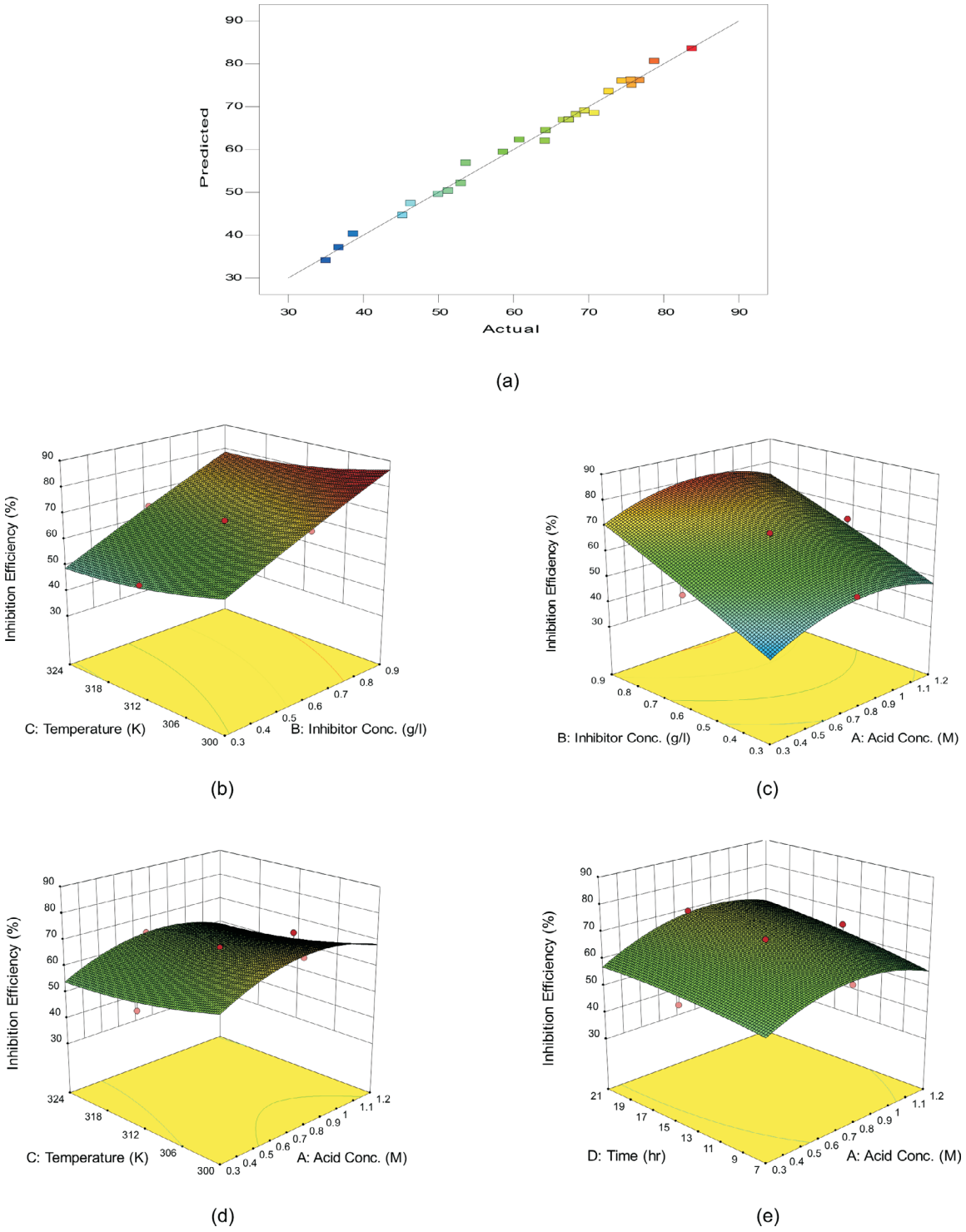

Figure 9 (**a**) Predicted *versus* actual plot, (**b**) Temperature/K *vs*. inhibitor conc./g L^{-1}, (**c**) inhibitor conc./g L^{-1} *versus* acid conc./M, (**d**) temperature/K *versus* acid conc./M and (**e**) time/h *versus* acid conc./M.

inhibition efficiency increased with increase in BKL concentration until it reached the optimum point. The increase in the BKL concentration expedites the formation of a dense film layer in the physical state.[12] However, the efficiency declined with increase in temperature, because an increase in temperature disorganizes the heterocyclic bonds of the extract. The temperature rise reduces the adsorption activity on the metal surface, especially when the mutual correlation between the metal and the inhibitor is quite low.[64] Fig. 9c shows the interactive influence of acid concentration and inhibitor concentration on the efficiency of the BKL. An increase in the inhibitor concentration reduces the corrosion of mild steel. This reduction may be attributed to the level of adsorption of polyphenols and heteroatoms of the BKL molecules which block the active sites of the steel surface from further activity, thereby giving an efficiency of 93 %. Fig. 9d shows the negative influence of temperature and acid concentration; increasing both variables reduces the efficiency of the BKL extract. Both factors may have created local anodes and cathodes on the surface, which increased the corrosion rate. In Fig. 9e, the effect of time and acid concentration was highlighted. An increase in the immersion time lowered the inhibition efficiency.

3.9.1. *Mathematical Model*

The mathematical model of the efficiency of the BKL extract as a function of the considered factors is expressed in terms of coded and actual factors. A quadratic model described the systematic connections between the inhibition efficiency and the factors of acid concentration (AC), inhibitor concentration (IC), temperature (T) and time (t). The coded factors were used to evaluate the response for given levels of each factor. By default, the maximum levels are fitted as +1, and the minimum levels are fitted as –1. The coded equation is useful in determining the impact of the factors. The analysis of variance (ANOVA) is presented in Table 10.

The model F-value of 130.92 implies that the model is significant and the BKL concentration dominated in this study, followed by temperature, time and acid concentration, respectively. There is only a 0.01 % chance that the F-value is large due to system agitation (noise). The noise may be assigned to flow rates of the bioactive constituents present in the BKL extract. Values of 'Prob> F' lower than 0.0500 indicate model terms are significant. Here A, B, C, D, AD, BC, BD, A^2 are significant model terms. Values higher than 0.1000 indicate the model terms are not significant. The 'Pred R-squared' of 0.9541 conforms strongly with the 'Adj R-squared' of 0.9843, and the variation is lower than 0.2. The coefficient of determination, R^2, depicts good statistical agreement between the observed and predicted values.[65] 'Adeq. precision' evaluates the signal to noise ratio. A ratio above 4 is adequately acceptable. The ratio of 43.14 indicates a good signal. This model can be used to navigate the design space. Accordingly, the quadratic regression model is adequate for predicting the inhibition efficiency of the BKL extract.

Coded factors

$$IE\% = +66.95+2.58*A+14.23*B-4.52*C+3.39*D-0.43*AB+0.054*AC+1.56*AD+0.58*BC-1.14*BD+0.12*CD-7.52*A^2-0.57*B^2+2.05*C^2-1.31*D^2 \quad (20)$$

Actual factors

$$IE\% = +1540.47743+53.32258*AC+14.52027*IC-9.38648*Temp+0.76456*Time\ 3.1667*AC*IC+9.95370E-003*AC.*Temp+0.49365*AC*Time+0.16181*IC.*Temp.-0.54345*IC.*Time+1.36905\ E-003*Temp*Time-37.13234*AC^2-6.32554*IC^2+0.014241*Temp^2-0.026822*Time^2 \quad (21)$$

Table 10 ANOVA for response surface quadratic model.

	Sum of squares	Degrees of freedom	Mean square	F-value	P-value Prob > F
Model	4813.78	14	343.84	130.92	<0.0001
A-Acid conc.	120.13	1	120.13	45.74	<0.0001
B-Inh. conc.	3644.30	1	3644.30	1387.5	<0.0001
C- Temp.	367.21	1	367.21	139.81	<0.0001
D-Time	207.33	1	207.33	78.94	<0.0001
AB	2.92	1	2.92	1.11	0.3081
AC	0.046	1	0.046	0.018	0.8962
AD	38.69	1	38.69	14.73	0.0016
BC	5.43	1	5.43	2.07	0.1710
BD	20.84	1	20.84	7.93	0.0130
CD	0.21	1	0.21	0.081	0.7804
A^2	146.49	1	146.49	55.78	0.0001
B^2	0.84	1	0.84	0.32	0.5801
C^2	10.90	1	10.90	4.15	0.0597
D^2	4.48	1	4.48	1.70	0.2114
Residual	39.40	15	2.63	–	–
Lack of fit	39.40	10	3.94	–	–
Pure error	0.000	5	0.000	–	–
Cor. total	4853.18	29	–	–	–
Std. deviation	1.62	–	–	–	–
Pre R-squared	–	–	0.9541	–	–
Adj R-squared	–	–	0.9843	–	–
Adeq. precision	–	–	43.148	–	–
CV %	–	–	2.59	–	–

3.10. Morphological Examination

Scanning electron microscopy was used to analyze the textural properties of the coupons in the unprotected and protected environment at magnifications of 1500 × 179 μm and 350 × 766 μm, respectively. Fig. 10a revealed the mild steel after 21 h of immersion in blank 1.2 M H_2SO4, while Fig. 10c showed the mild steel immersed in 1.2 M H_2SO_4/0.9g L^{-1} BKL. In the blank solution, coarse and uneven surface fractions[66] were noticed with various macro-pores (Fig 10b). The corrosion topography was visible enough due to the hostile nature of chloride and sulphate ions in the facial dissolution layer of the steel.[67] The micrography of mild steel in the inhibited solution (Fig.10c,d) evidently differs

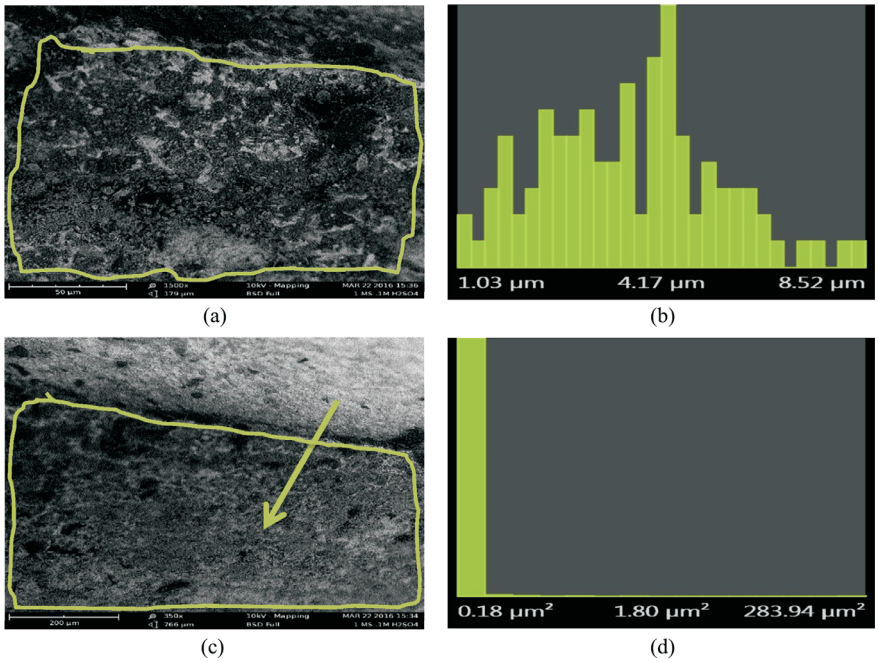

Figure 10 SEM/pore histogram of mild steel in (**a**–**b**) blank electrolyte and (**c**–**d**) inhibited medium.

from the control sample in 1.2 M H_2SO_4. The level of iron oxide formed was surpressed due to the physical formation of a dense film on the facial layer of the steel.[68] The high activity of BKL on the mild steel surface is highly dependent on the concentration of the studied inhibitor.

4. Conclusions

The adsorption of the BKL extract on the mild steel surface is best fitted by the Langmuir isotherm. Polarization measurements signify that the inhibitor (BKL extract) greatly impeded both cathodic and anodic side-reactions. Also, quantum chemical studies predicted the feasible adsorption areas of BKL. Molecular simulation results revealed that BKL molecules assumed a flat adsorption orientation with respect to the mild steel surface. From the optimization studies, the quadratic model adequately expressed the relationship between the inhibition efficiency and the considered factors of the inhibition process. The surface examination showed the occurrence of a film layer at the metal solution interface. The experimental and theoretical results are in agreement that BKL extract is a viable corrosion inhibitor of mild steel in H_2SO_4 electrolyte.

Compliance with ethical standards

Conflict of interest: The authors declare that they have no conflict of interest.

Funding

This research received no external funding.

[§]ORCID iD

V.C. Anadebe: orcid.org/0000-0002-7559-446X

References

1 Y. Liangtian, M. Zhang, C. Shidong, T. Yunji and W. Haixia, Investigation of corrosion effect of *enprofylline* drug on mild steel corrosion in sulphuric acid, *Int. J. Electrochem. Sci.*, 2020, **15**, 5102–5114.

2 T.L. Roland and O. Oluwatobilola, Corrosion inhibition properties of the combined admixture of essential oil extracts on mild steel in the presence of SO_4^{2-}anions, *S. Afr. J. Chem. Engr.*, 2018, **26**, 35–41.

3 E.E. Oguzie, Z.O. Iheabunike, K.L. Oguzie, C.E. Ogukwe, M.A. Chidiebere, C.K Enenebeaku and C.O. Akalezi, Corrosion inhibiting effect of *Aframomum meleguta* extracts and adsorption characteristics of the active constituents on mild steel in acidic media, *J. Dispersion Sci. Tech.*, 2013, **34**, 516–527.

4 A. Dehghani, G. Bahlakeh, B. Ramezanzadeh and M. Ramezanzadeh, Electronics/atomic level fundamental theoretical evaluations combined with electrochemical/surface examinations of *Tamarindus indiaca* aqueous extract as a new green inhibitor for mild steel in acidic solutions (HCl 1 M), *J. Taiwan Inst. Chem. Eng.*, 2019.
DOI: 10.1016/j.jtice.2019.05.006

5 N. Asadi, M. Ramezanzadeh, G. Bahlakeh and B. Ramezanzadeh, Utiizing lemon balm extract as an efficient green corrosion inhibitor for mild steel in 1 M HCl solution: a detailed experimental, molecular dynamics, Monte Carlo and quantum mechanics study, *J. Taiwan Inst. Chem. Eng.*, 2019, **95**, 252–272.

6 Z. Sanaei, M. Ramezanzadeh G. Bahlakeh and B. Ramezanzadeh, Use of *Rosa canina* fruit extract as a green corrosion inhibitor for mild steel in 1 M HCl solution, a complementary experimental, molecular dynamics and quantum mechanics investigation, *J. Ind. Eng. Chem.* 2019, **69**, 18–31.

7 Y. Lekbach, L. Zhong, D. Xu, S. El-Abed, Y. Dong, D. Liu, G. Tingyue, S.I. Koraichi, K.E. Yang and F. Wang, *Salvia officinalis* extract mitigates the microbiologically influenced corrosion of 304L stainless steel by *Pseudomonas aeruginosa* biofilm, *Bioelectrochem.*, 2019, **128**, 193–203.

8 A. Saxena, D. Prasad and R. Haldhar, Investigation of corrosion inhibition effect and adsorption activities of *Custcuta reflexa* extract for mild steel in 0.5 M H_2SO_4, *Bioelectrochem.*, 2019, **124**, 156–164.

9 Q. Wang, B. Tan, H. Bao, Y. Xie, Y. Mou, P. Li, D. Chen, Y. Shi, X. Li and W. Yang, Evaluation of *Ficus tikoua* leaves extract as an eco-friendly corrosion inhibitor for carbon steel in HCl media, *Bioelectrochem.*, 2019, **128**, 49–55.

10 A. Dehghani, G. Bahlakeh and B. Ramezanzadeh, A detailed electrochemical/theoretical exploration of the aqueous chinese goose berry fruit shell extract as a green and cheap corrosion inhibitor for mild steel in acidic solution, *J. Mol. Liq.*, 2019, **282**, 366–384.

11 S.E. Haddadi, E. Alibakhshi, G. Bahlakeh, B. Ramezanzadeh and M.A. Mahdavian, Detailed atomic/level computational and electrochemical exploration of the *Juglans regia* green fruit shell extract as a sustainable and highly efficient green corrosion inhibitor for mild steel in 3.5 w % of NaCl solution, *J. Mol. Liq.*, 2019, **284**, 682–699.

12 G. Bahlakeh, B. Ramezanzadeh, A. Dehghani and M. Ramezanzadeh, Novel cost effective and high performance green inhibitor based on aqueous *Peganum harmala* seed extract for mild steel corrosion in HCl solution: detailed experimental and electronic/atomic level computational exploration, *J. Mol. Liq.*, 2019, **283**, 174–195.

13 V.C. Anadebe, O.D. Onukwuli, M. Omotioma and N.A. Okafor, Experimental, theoretical modeling and optimization of inhibition efficiency of pigeon pea leaf extract as anti-corrosion agent of mild steel in acid environment, *Mater. Chem. Phys.*, 2019, **233**, 120–132.

14 P.C. Okafor, V.I. Osabor, and E.E. Ebenso, Eco-friendly corrosion inhibitors: inhibitive action of ethanol extracts of *Garcinia kola* for the corrosion of mild steel in H_2SO_4 solutions, *Pigment Resin Tech.*, 2007, **36**(5), 299–30.

15 E.E. Oguzie, K.L. Iyeh and A.I. Onuchukwu, Inhibition of mild steel corrosion in acidic media by aqueous extracts from *Garcinia kola* seed, *Bull. Electrochem.*, 2006, **22**(2), 63–68.

16 N.O. Eddy, Adsorption and inhibitive properties of ethanol extract of *Garcinia kola* and *Cola nitida* for the corrosion of mild steel in H_2SO_4, *Pigment Resin Tech.*, 2010, **39**(6), 348–354.

17 E.E. Oguzie and A.I. Onuchukwu, Inhibition of mild steel corrosion in acidic media by aqueous extracts from *Garcinia kola* seed, *Corros. Rev.*, 2007, **25**(3-4), 355–362.

18 A.I. Ikeuba, P.C. Okafor, U.J. Ekpe and E.E. Ebenso, Alkaloid and non-alkaloid ethanolic extracts from seeds of *Garcinia kola* as green corrosion inhibitors of mild steel in H_2SO_4 solution, *Int. J. Electrochem. Sci.*, 2013, **8**, 7455–7467.

19 E.E. Oguzie, Evaluation of the inhibitive effect of some plant extracts on the acid corrosion of mild steel, *Corros. Sci.*, 2008, **50**, 2993–2998.

20 V.C. Anadebe, O.D. Onukwuli, M. Omotioma and N.A. Okafor, Optimization and electrochemical study on the control of mild steel corrosion in hydrochloric acid solution with bitter kola leaf extract as inhibitor, *S. Afr. J. Chem.*, 2018, **71**, 51–61.

21 A.O. Jelili, T.A. Olaniyi, G.A. Emmanuel, H.A. Kehinde, I.O. Bayonle, I.A. Bolanle and C.H. Donavon, In vitro and in vivo biochemical evaluations of the methanolic leaf extract of garcina kola, *International Scholarly Research Notices*, 2014, Article ID **391692**:
http://dx.doi.org/10.1155/2014/391692

22 B. Jeetendra, P.K. Jain and J. Preeti, Experimental and computational studies of *Nicotiana tabacum* leaves extract as green corrosion inhibitor for mild steel in acidic medium, *Alexandria Eng. J.*, 2015, **54**, 769–775.

23 M. Omotioma and O.D. Onukwuli, Modeling the corrosion inhibition of mild steel steel in HCl medium with the inhibitor of pawpaw leaves extracts, *Portugalie Electrochim. Acta*, 2016, **34**, 287–294.

24 N. Nagm, N.G. Kandile, E.A. Badr and M.A. Mohammed, Gravimetric and electrochemical evolution of environmentally friendly nonionic corrosion inhibitors for carbon steel in 1 M HCl, *Corros. Sci.*, 2012, **65**, 94–103.

25 K.B. Pandey and S.I. Rizvi, Plant polyphenols as dietary anti-oxidant in human health and disease, *Oxid. Med. Cell Longev.*, 2009, **2**, 270–278.

26 S. Kumar and Pandey A.K. Chemistry and biological activities of flavonoids: an overview. *Sci. World J.*, 2013, 162750.

27 D. Prakash, S. Suri, G. Upadhyay and B.N. Singh, Total phenol, antioxidant and free radical scavengaing activities of some medicinal plants, *Int. J. Food Sci. Nutr.*, 2007, **58**, 18–28.

28 S. Panda, A. Kar, P. Sharma and A. Sharma, Cardio-protective potentials of N, α-L-rhamnopyranosyl vincosamide, an indole alkaloid isolated from the leaves of *Moringa oleifera* in isoproterenol induced cardiotoxic rats: in vivo and in vitro studies, *Bioorg. Med. Chem. Lett.*, 2013, **23**, 959–962.

29 P. Sahakitpichan, C. Mahidol, W. Disadee, S. Ruchirawat and T. Kanchanapoom, Unusual glycosides of pyrrole alkaloid and 4'-hy-

droxyphenylethanamide from leaves of *Moringa oliefera*, *Phytochem.*, 2011, **72**, 791–795.

30 J.M. Augustin, V. Kuzina, S.B. Andersen and S. Bak, Molecular activities, biosynthesis and evolution of triterpeniod saponins, *Phytochem.*, 2011, **72**, 435–457.

31 S.A. Umoren, U.M. Eduok, M.M. Solomon and A.P. Udoh, Corrosion inhibition by leaves and stem extracts of *Sida acuta* for mild steel in 1M H_2SO_4 solutions investigated by chemical and spectroscopic techniques, *Arab. J. Chem.*, 2016, **9**, S209–S224.

32 U.M. Eduok, S.A. Umoren and A.P. Udoh, Synergistic inhibition effects between leaves and stem extracts of *Sida acuta* and iodide ion for mild steel corrosion in 1 M H_2SO_4 solutions, *Arab. J. Chem.*, 2012, **5**, 25–337.

33 C.S. Okafor, O.D. Onukwuli and V.C. Anadebe, Optimization and impedance study on the inhibition efficiency of moringa leaf extract as corrosion inhibitor of aluminum in alkaline medium, *Pharm. Chem. J.*, 2019, **6**(3), 53–62.

34 T.L. Roland and B. Philip, Electrochemical analysis of SiC composite additions at 7.5 % weight content on the corrosion resistance of monolithic aluminum alloy in sulphate-chloride solution, *J. Mater. Res. Tech.*, 2019, **8**(3), 2517–2527.

35 T.L. Roland, Surface coverage and corrosion inhibition effect of *Rosmarinus officinalis* and zinc oxide on the electrochemical performance of low carbon steel in dilute acid solutions, *Results Phys.*, 2018, **8**, 172–179.

36 T.L. Roland and A.L. Celophas, Anti-corrosion properties of the symbolic effect of *Rosmarinus officinalis* and trypsin complex on medium carbon steel, *Results Phys.*, 2018, **10**, 99–106.

37 S.Y. Aprael, A.A. Khadom and K.W. Rafal, Apricot juice as green corrosion inhibitor of mild steel in phosphoric acid, *Alexandria Eng. J.*, 2013, **52**,129–135.

38 M.A. Chidiebere, E.E. Oguzie, L. Liu, L. Ying and F. Wang Inhibitory action *Funtumia elastica* extracts on the corrosion of Q235 mild steel in HCl acid medium: experimental and theoretical studies, *J. Dispersion Sci. Tech.*, 2015, **36**, 1115–1125.

39 Y. Qiang, Z. Shengtao, T. Bochuan and C. Shijin, Evaluation of ginkgo leaf extract as an eco-friendly corrosion inhibitor of X70 steel in HCl solution, *Corros. Sci.*, 2018, **133**, 6–16.

40 A. Dehghani, G. Bahlakeh, B. Ramezanzadeh and M. Ramezanzadeh, Detailed macro-/micro scale exploration of the excellent active corrosion inhibition of a novel environmentally friendly green inhibitor for carbon steel in acidic environment, *J. Taiwan Inst. Chem. Eng.*, 2019, **100**, 239–261.

41 A. Popova, E. Sokolova, S.M. Raicheva and M. Christov M, AC and DC study of the temperature effect on mild steel corrosion in acid media in the presence of benzimidazole derivatives, *Corros. Sci.*, 2003, **45**, 33–58.

42 H. Ashassi-Sorkhabi, D. Seifzadeh and M.G. Hosseini, EIS and polarization studies to evaluate the inhibition effect of 3H-phenothiazi in -3-one, 7-dimethylamin on mild steel corrosion in 1M HCl solution, *Corros. Sci.*, 2008, **50**, 3363–3370.

43 F.S. De souza and A. Spinelli, Caffeic acid as a green corrosion inhibitor for mild steel, *Corros. Sci.*, **51**, 642–649.

44 L.G. Da Trindade and R.S. Goncalves, Evidence of caffeine adsorption on low carbon steel surface in ethanol, *Corros. Sci.*, 2009, **51**, 1543–1578.

45 A. Dehghani, G. Bahlakeh, B. Ramezanzadeh and M. Ramezanzadeh M, Potentials of borage flower aqueous extract as an environmentally sustainable corrosion inhibitor for acid corrosion of mild steel: electrochemical and theoretical, *J. Mol. Liq.*, 2019, **277**, 895–911.

46 J.C. Da Rocha, D. Cunha Poniciano Gomes and E.D. Elia, Corrosion inhibition of carbon steel in HCl solution by fruit peel aqueous extract, *Corros. Sci.*, 2010, **52**, 2341–2348.

47 M. Lebrini, F. Robert, A. Lecante and C. Roos, Corrosion inhibition of C38 steel in 1M HCl acid medium by alkaloids extract from *Oxandra asbecki* plant, *Corros. Sci.*, 2010, **53**, 687– 695.

48 M.A. Chidiebere, E.E. Oguzie, L. Liu, L. Ying and F. Wang, Corrosion inhibition of Q235 mild steel in 0.5 M H_2SO_4 solution by phytic acid and synergistic iodide additives, *Ind. Eng. Chem. Res.*, 2014, **53**, 7670–7679.

49 M.A. Chidiebere, C.E. Ogukwe, K.L. Oguzie, C.N. Eneh and E.E. Oguzie, Corrosion inhibition and adsorption behavior of *Punica granatum* extract on mild steel in acidic environments: experimental and theoretical studies, *Ind. Eng. Chem. Res.*, 2012, **51**, 668–677.

50 M.A. Chidiebere, E.E. Oguzie, L. Liu, L. Ying and F. Wang, Adsorption and corrosion inhibiting effect of riboflavin on Q235 mild steel corrosion in acidic environments. *Mater. Chem. Phys.*, 2015, **156**, 95–104.

51 M. Al-Sabagh, N. Gh-Kandile, N.M. Nasser, E. Olfat and A. El-Azabawy, Investigation of electro and quantum chemical properties of some novel cationic surfactants based on 1,3,5-triethanolhexahydro-1, 3, 5-triazine as corrosion inhibitors for CS in hydrochloric acid, *Chem. Eng. Comm.*, 2014.
DOI: 10.1080/00986445.2014.926452

52 F. Jia-Jun, L. Su-ning, L. Cao, Y. Wang, L. Yan and L. Lu-De, L-Tryptophan as green corrosion inhibitor for low carbon steel in hydrochloric acid solution, *J. Mater. Sci.*, 2010, **45**, 979–986.

53 F. Jia-Jun, L. Su-ning, Y. Wang, L. Xiao-Dong and L. Lu-De, Computational and electrochemical studies on the inhibition of corrosion of mild steel by L-cysteine and its derivatives, *J. Mater. Sci.*, 2011, **46**, 3550–3559.

54 F.E. Abeng, M.E. Ikpi, V.E. Okpashi, O.A. Ushie and M.E. Obeten, Electrochemical and quantum chemical parameter of (-)-(s)-9-Fluoro-2,3-dihydro-3-methyl-10-(4-methyl-1-piperazinyl)-7-oxo-7H -pyrido[1,2,3-de]-1,4-benzoxazine-6-carboxylic acid as anti-corrosive agent for API 5L X-52 steel, *J. Electrochem. Sci. Eng.*, 2020, **10**(3), 235–244.

55 M.E. Ikpi and F.E. Abeng, Theoretical study on the structural effect of benzoxazin derivatives as corrosion inhibitor for carbon steel in acid media, *Chem. Sci. Transaction*. 2017, **6**(4), 569–576.

56 E.E. Oguzie, S.G. Wang, Y. Li and F.H. Wang, Influence of iron microstructure on corrosion inhibitor performance in acidic media, *J. Phys. Chem.*, 2009, **113**, 8420–8429.

57 K.F. Khaled, Studies of iron corrosion inhibition using chemical, electrochemical and computer simulation techniques, *Electrochim. Acta*, 2010, **55**, 6523–6532.

58 K.F. Khaled, Guanidine derivatives as a new corrosion inhibitor for copper in 3% NaCl solution, *Mater. Chem. Phys.*, 2008, **112**, 104–111.

59 F. Jia-Jun, L. Su-ning, Y. Wang, L. Cao and L. Lu-De, Computational and electrochemical studies of some amino acid compounds as corrosion inhibitor for mild steel in hydrochloric acid solution, *J. Mater. Sci.*, 2010, **45**, 6255–6265.

60 F.E. Abeng, M.E. Ikpi, O.A. Ushie and M.M. Edim, Investigation of inhibition effect of nifedipine on API 5L X-52 steel corrosion in hydrochloric acid, *J. Chem. Soc. Nig.*, 2019, **44** (6) 1132–1141.

61 M.E. Ikpi and F.E. Abeng, Electrochemical and quantum chemical investigation on adsorption of nifedipine as corrosion inhibitor at API 5L X-52 steel/ HCl acid interface, *Arch. Metall. Mater.*, 2020, **65**(1), 125–131.

62 C.S. Okafor, V.C. Anadebe and O.D. Onukwuli, Experimental, statistical modeling and molecular dynamics simulation concept of *Sapium ellipticum* leaf extract as corrosion inhibitor for carbon steel in acid environment, *S. Afr. J. Chem.*, 2019, **72**, 164–175.

63 O.D. Onukwuli, V.C. Anadebe and C.S. Okafor, Optimum prediction for inhibition efficiency of *Sapium ellipticum* leaf extract as corrosion inhibitor of aluminum alloy (AA3003) in HCl solution using electrochemical impedance spectroscopy and response surface methodology, *Bull. Chem. Soc. Ethiop.*, 2020, **34**(1), 175–191.

64 A.S. Yaro, A.A. Khadom and R.K. Wael, Garlic powder as a safe environment green corrosion inhibitor for mild steel in acidic media; adsorption and quantum chemical studies, *J. Chinese Chem. Soc.*, 2014, **61**, 615–623.

65 P. Sharma, L. Singh and N. Dilbagh, Optimization of process variables for decolourization of disperse yellow 211 by *Bacillus subtiles* using Box-Behnken design, *J. Hazard. Mater.*, 2009, **164**, 1024–1029.

66 C.A. Loto, R.T. Loto and O.J. Olufunmilayo, Effect of benzamide on the corrosion inhibition of mild steel in sulphuric acid, *S. Afr. J. Chem.*, 2017, **70**, 38–43.

67 R.T. Loto, C.A. Loto and A.P. Popoola, Inhibition effect of deanol on mild steel corrosion in dilute sulphuric acid, *S. Afr. J. Chem.*, 2015, **68**, 105–114.

68 P. Singh, C.D. Singh, K. Srivastava, V. Srivastava and M.A. Quraishi, Expired atorvastatin drug as corrosion inhibitor for mild steel in hydrochloric acid solution, *Int. J. Ind. Chem.*, 2015, **8**, 363–372.